Enthalpy Recovery of PMMA/Silica Nanocomposites

ARTICLE *in* MACROMOLECULES · AUGUST 2010

Impact Factor: 5.8 · DOI: 10.1021/ma101217y

Accelerated physical aging in PMMA/silica nanocomposites

Virginie M. Boucher,*[a] Daniele Cangialosi,[b] Angel Alegría,[bc] Juan Colmenero,[abc] Juan González-Irun[d] and Luis M. Liz-Marzan[d]

Received 4th February 2010, Accepted 30th March 2010
First published as an Advance Article on the web 26th May 2010
DOI: 10.1039/c001656j

We have monitored the physical aging process below the glass transition temperature (T_g) of poly(methyl methacrylate) PMMA/silica nanocomposites by means of broadband dielectric spectroscopy (BDS). To do so, we have followed the evolution with time of the dielectric strength of the PMMA secondary relaxation process that dominates the dielectric response overall below T_g. The employed silica particles are spherical and present a diameter of several hundred nanometres. We have investigated polymer nanocomposites with silica concentration of about 10% wt. This results in an interparticle distance of the order of several hundred nanometers. Despite the general similarity between the segmental dynamics of the nanocomposites and that of pure PMMA as evidenced by both differential scanning calorimetry (DSC) and BDS experiments, the former systems display markedly accelerated physical aging in comparison to the pure polymer. This striking result suggests that the relevant length scale of the system under investigation plays a crucial role in affecting the mechanism of the physical aging process. As a natural consequence of such evidence, the diffusion of free volume holes—annihilating at the "external surface" of the polymer being aged—has been invoked to explain the strong mismatch between the physical aging in the nanocomposite and that of pure PMMA. Such an interpretation is discussed in light of the recent results on physical aging of polymer nanocomposites.

I. Introduction

In recent years, the possibility of adding nanofillers into a polymer matrix has emerged as a very promising method for improving the initial properties. Synergy on a molecular level between the physical and chemical properties of inorganic and organic components is expected to act favourably on the macroscopic properties and is the main driving force in the research of novel inorganic-polymeric nanocomposites. These materials frequently show improved properties, such as enhanced mechanical strength, thermal stability, or higher chemical resistance, which are useful characteristics for emergent technological applications.[1–4]

Among the possible aspects related to the study of polymer nanocomposites, the slow evolution of thermodynamic properties (enthalpy, volume *etc.*) towards equilibrium, known as physical aging, occurring below the glass transition temperature (T_g) of the polymer is certainly one of the most intriguing facets.[5,6] The kinetics of such evolution is intimately related to the molecular mobility[7] in the glassy state.[5,6] Thus, the understanding of physical aging from a fundamental point of view is a key aspect in glass science. Apart from the fundamental implications, physical aging may result in many deleterious effects ranging from embrittlement to reduction in permeability and dimensional instability. That is the reason why this phenomenon has been extensively studied for bulk polymer systems in the past years.[5]

Despite the large body of work in polymer nanocomposites, to the best of our knowledge, so far only few studies reporting on the time-dependence of the properties of such materials have been presented.[8] In the case of polymer nanocomposites and, more generally, nanoscale confined materials such as polymer thin films or polymers in nanopores, the physical aging process can be dramatically modified in comparison to the same process in bulk polymers. This is due to the fact that nanoscale confinement may induce two kinds of effects on polymer segmental mobility: i) one is due to the fact that molecular mobility in glass-forming systems is generally associated with a typical length scale[9] and the presence of a physical barrier in confined materials may modify the size and the temperature dependence of such a length scale;[10,11] ii) the other is the surface effect, responsible for mobility changes at the interface: polymer-nanoparticle in nanocomposites; polymer-matrix in nanoporous materials; polymer-air or substrate in thin films.[12–16] These peculiarities of physical aging in nanoscale confined polymers explain the emerging interest of the scientific community in the subject.[17–34]

So far, the studies of physical aging in confined systems have shown quite contradictory results. On one hand, in systems presenting a typical length scale of the order of nanometres, a reduction, or even suppression, of physical aging has been reported,[20,21,25,34] with the only exception of glassy *o*-terphenyl (OTP) confined in nanopores that is reported to display accelerated physical aging.[18] On the other hand, in systems with

[a]*Donostia International Physics Center, Paseo Manuel de Lardizabal 4, 20018 San Sebastián, Spain. E-mail: sckboucv@.ehu.es*
[b]*Centro de Física de Materiales Centro Mixto (CSIC-UPV/EHU), Apartado 1072, 20080 San Sebastián, Spain*
[c]*Departamento de Física de Materiales, Universidad del País Vasco (UPV/EHU), Apartado 1072, 20080 San Sebastián, Spain*
[d]*Universidad de Vigo, Deptartamento de Química Física Unidad Asociada CSIC, 36310 Vigo, Spain*

a typical length scale of several hundred nanometres or larger, an acceleration of physical aging has been observed.[17,24,27,30,35–39] The full comprehension of these results is currently a matter of debate within the scientific community and still needs to be elucidated. Furthermore, the confinement-induced changes in the physical aging process, whether an acceleration or a reduction is observed, cannot always be explained by changes in the overall molecular mobility (and therefore in the T_g). In particular, deviations from the bulk aging rate are observed at length scales of confinement which are far too large to induce any change in the molecular mobility as a result of either finite size[9,40,41,42] or interfacial effects.[43,44,45]

As far as polymer thin films of the order of several hundred nanometers thick are concerned, the acceleration of physical aging in comparison to the bulk polymer has been explained invoking a mechanism based on diffusion of free volume holes and their annihilation at the external surface.[27,35–38] The idea of a diffusion mechanism for physical aging has been considered since long ago. In the early 1940s, Alfrey *et al.*[46] proposed that diffusion of free volume holes and their annihilation at the external surface of the sample could be responsible for the time evolution of the macroscopic thermodynamic properties. This idea was abandoned during several decades after Kovacs' experiments in powdered polystyrene (PS) *i.e.* with relatively large external surface, which did not display any accelerated physical aging in comparison to the bulk polymer.[47] It is worth mentioning that in this case the typical size of the powdered PS was of the order of 10 μm. More recently, the diffusion mechanism was proposed again by several studies[48,49] that successfully modelled the volume recovery of poly(vinyl acetate) (PVAc) through a diffusion mechanism.

An alternative explanation for the acceleration of physical aging in thin films has been very recently provided by Rowe *et al.*,[50] measuring the free volume at different distances from the film surface by means of variable energy positron annihilation. They suggested that the acceleration of physical aging in polysulfone thin films has to be attributed to the enhanced molecular mobility near the film surface.[50]

To clarify the possible origin of the change in the rate of physical aging in confined polymer systems, in this work we study poly(methyl methacrylate)/silica (PMMA/silica) nanocomposites by means of broadband dielectric spectroscopy (BDS) and differential scanning calorimetry (DSC). Silica nanoparticles displaying different diameters and surface treatments were used to prepare the nanocomposites *via* in situ polymerization of methyl methacrylate (MMA). The dynamics of the pure polymer and the nanocomposites were assessed by using DSC and BDS. The physical aging of nanocomposites was conveniently followed monitoring the change of the dielectric relaxation strength of the PMMA secondary relaxation that dominates the dielectric response of this polymer both below and above T_g.[51]

In these samples, although the molecular mobility was shown to remain unmodified after the addition of silica particles to PMMA, the physical aging was revealed to be faster in the presence of silica nanoparticles. Moreover, the aging rate was shown to be independent of the particles surface treatment, but only dependent on the ratio between the particle surface and the volume of PMMA. These results can be explained through a diffusion model describing physical aging of a polymer as the diffusion of free volume holes towards polymer interfaces.

II. Experimental

Chemicals

NH_4OH (32%), tetraethylorthosilicate (TEOS) and 3-(trimethoxysilyl)propyl methacrylate (TPM), octadecyltrimethoxysilane (OTMS), 2,2-dimethoxy-2-phenylacetone (DMPA) and methyl methacrylate (MMA) were purchased from Aldrich. All chemicals were used as received. Pure grade ethanol, pure grade chloroform and Milli-Q grade water were used in all preparations.

Preparation of the pure polymer and polymer nanocomposites

Silica particles with diameters of 200 and 350 nm were prepared as described elsewhere using a variation of the Stöber method.[52] Surface modification was carried out for hydrophobization of silica surfaces using silane coupling agents. Thus, 350 nm silica particles were functionalized using two different silane coupling agents. One treatment was performed by adding 3 mL of 3-(trimethoxysilyl)propyl methacrylate (TPM) to 100 mL of 0.3 M silica dispersion at room temperature.[53] After 30 min 30 mL solvent was slowly distilled off for 2 h under stirring and finally the sample was cleaned by repeated centrifugation and transferred into chloroform. Concerning the other treatment, 10 mL of 10% octadecyltrimethoxysilane (OTMS) chloroform solution was added in a dispersion of particles in ethanol (100 mL of 0.3 M) in the presence of ammonia (1 M).[54] Grafting was achieved by hydrolysis of methoxy groups and condensation of the resulting silane triols with surface Si-OH groups. After 24 h, the particles were separated by centrifugation, washed with ethanol and then dispersed in chloroform. In the case of particles with a diameter of 200 nm, only TPM was employed as surface modifier following the same procedure as described above.

Final samples were prepared as described elsewhere.[55] Briefly, a certain amount of the photoinitiator DMPA (2,2-dimethoxy-2-phenylacetone) was dissolved in a silica-MMA dispersion (final DMPA concentration 0.25 wt%), followed by injection in 20 × 5 × 1 mm glass cells made by gluing two glass slides spaced by a Teflon with adhesive tape. The cell was irradiated with UV light inside a commercial photoreactor (Luzchem LZC-UV) containing 16 UV fluorescent tubes (8 W) for 6 h to achieve complete polymerization of PMMA. The so-obtained materials, listed in Table 1, were compression moulded at 60 °C above PMMA T_g, to obtain 0.2 mm thick films.

Characterization of the samples

Molecular weight and polydispersity index of PMMA were assessed in all samples, by means of gel permeation chromatography (GPC) measurements.

The weight fraction of silica particles in the nanocomposites samples was measured by thermogravimetric analyses (TGA), on a thermogravimeter TA Q-500, with a heating ramp of 10 °C/min up to 750 °C under flowing nitrogen (20 cm^3 min^{-1}). The molecular weight of PMMA and its distribution, together with the weight fraction of silica particles are summarized in Table 1.

Table 1 Summary of PMMA and PMMA nanocomposite characteristics: silica weight fraction, silica particle diameter, interparticle distance, PMMA molecular weight, polydispersity index

Sample	Silica weight fraction, W_f (%)	Surface treatment	Particle diameter (nm)	Interparticle distance, l (nm)	PMMA M_w (kg mol^{-1})	M_w/M_n
PMMA	—	—	—	—	880	4
A10	8.9	TPM	350	1410	877	4
R10	8.9	OTMS	350	1410	760	4
V10	8.9	TPM	200	806	830	4

According to the values reported in this table, both the silica particle weight fraction and the molecular weight of PMMA are, within experimental error, equal in all samples.

TEM measurements were performed using a high-resolution transmission electron microscope TECNAI G2 20 TWIN. The measurements were carried out using an accelerating voltage of 200 kV, under low dose conditions. Nanocomposites ultra-thin sections of about 70 nm were cut by a LEICA EM UC6 microtome equipped with a diamond knife and placed on a 400-mesh copper grid.

Thermal analyses of the samples were carried out by means of the differential scanning calorimeter (DSC) (DSC-Q2000) from TA Instruments. The temperature was calibrated with melting indium. All DSC measurements were performed under nitrogen atmosphere on samples of about 10 mg. Hermetic aluminium pans were used for all the materials. In order to erase their previous thermal history, all samples were first heated to 150 °C at a heating rate of 20 °C min^{-1}, and subsequently cooled to room temperature at a cooling rate of 10 °C min^{-1} for data collection.

A broadband dielectric spectrometer, Novocontrol Alpha analyzer, was used to measure the complex dielectric function, $\varepsilon^*(\omega) = \varepsilon'(\omega) - i\cdot\varepsilon''(\omega)$, in the frequency ($f = \omega/2\pi$) range from $f = 10^{-2}$ Hz to $f = 10^7$ Hz. The samples were placed between parallel gold-plated electrodes (without spacers to allow dimensional changes during aging) with a diameter of 20 mm. The sample thickness was typically 0.2 mm. The capacitor assembly was kept in a nitrogen cryostat, with a temperature stability better than ±0.1 K over the duration of the experiments. Broadband dielectric spectroscopy was employed to characterize the dynamics of PMMA both pure and in the nanocomposites and to probe physical aging. As far as the characterization of the dynamics is concerned, samples were measured after quenching in liquid nitrogen in isothermal frequency scans recording $\varepsilon^*(\omega)$ every 5 K over the temperature range of 273–423 K. No effect of the thermal history was found on the typical relaxation time of PMMA, identified with the time corresponding to the maximum of the loss peak of the permittivity.

The physical aging of the samples was monitored by following the time evolution of the complex dielectric function $\varepsilon^*(\omega)$, which was measured continuously at the annealing temperature T_a. Prior to any measurement, the samples were firstly rejuvenated at a temperature corresponding to T_g + 30 K, for 5 min, and subsequently quenched in liquid nitrogen. Then, the temperature of the samples was increased to the selected annealing temperature. A time of about 10 min was required for accurate temperature stabilization. The selected aging temperatures ranged from 303 to 353 K with an interval of 10 K. In order to quantify the extent of physical aging, the complex dielectric function associated with the PMMA secondary relaxation process was fitted by the Havriliak-Negami (HN) function:[56]

$$\varepsilon^*(\omega) = \varepsilon_\infty + \frac{\Delta\varepsilon}{\left[1 + (i\omega\tau_{HN})^{\alpha_{HN}}\right]^{\gamma_{HN}}} \quad (1)$$

where ε_∞ is the high frequency limit value of the dielectric constant, $\Delta\varepsilon$ is the dielectric strength of the relaxation process, τ_{HN} is the HN relaxation time, and α_{HN} and γ_{HN} are the shape parameters of the HN function describing respectively the symmetric and asymmetric broadening of the complex dielectric permittivity. During the course of physical aging, a decrease of the $\Delta\varepsilon$ was observed, whereas τ_{HN}, α_{HN} and γ_{HN} remained constant. Thus $\Delta\varepsilon$ associated with the PMMA β-process represents a robust parameter to monitor physical aging in glassy PMMA.

III. Results

A. Characterization of the pure polymer and polymer nanocomposites

The TEM micrographs of all investigated PMMA/silica nanocomposites are presented in Fig. 1. TEM analysis of the PMMA/silica samples reveals well dispersed silica particles in samples A10 and V10. On the other hand, the dispersion of silica particles in R10 is not as homogeneous as in A10 and V10. Nonetheless this does not result in a decrease in the particles surface/volume of PMMA ratio, since the silica particles do not aggregate significantly. This means that the surface treatment of the silica particles with TPM is particularly effective to avoid aggregation—probably due to the fact that TPM chemically takes part in MMA polymerization—whereas the one with OTMS, although not as effective as the former treatment, limits significant aggregation of silica particles.

In Fig. 1, the difference in the diameter of the silica particles contained in the sample V10 in comparison to the samples A10 and R10, is clearly visible. Furthermore, the TEM images of PMMA nanocomposites show a shorter interparticle distance in the sample V10, in comparison with the samples A10 and R10. The observed interparticle distances are in agreement with the theoretical ones, reported in Table 1 and calculated according to the following equation:

$$l = d\left[\left(\frac{\pi}{6V_f}\right)^{1/3} - 1\right] \quad (2)$$

where V_f is the volume fraction of silica and d is the diameter of silica particles. The volume fraction V_f of the silica particles in the composite is determined, for the known filler weight content W_f (reported in Table 1), according to the expression:

$$V_f = \frac{W_f\rho_m}{W_f\rho_m + (1 - W_f)\rho_f} \quad (3)$$

where ρ_m and ρ_f are the densities of the matrix and filler, equal to 1.16 and 2.65 g cm^{-3}, respectively; herein, the subscripts "m" and "f" refer to the characteristics of the matrix and filler, respectively.

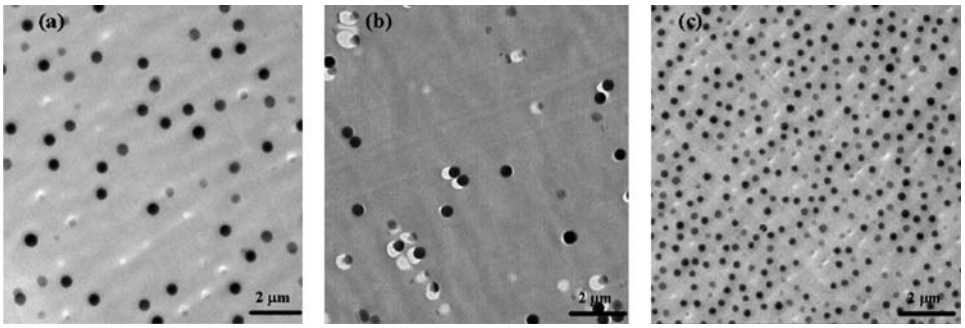

Fig. 1 TEM images of the PMMA/silica nanocomposites: A10 (a), R10 (b), and V10 (c).

To conclude this section, the following results can be highlighted: i) neither the molecular weight of PMMA nor its distribution are significantly affected by the presence of silica particles during the polymerization process; ii) all nanocomposites display the same silica weight fraction; iii) the silica particles are generally well dispersed in all nanocomposites. The latter result implies that the nanocomposite with smaller silica particles (V10) presents a shorter interparticle distance in comparison with the other nanocomposites (A10 and R10).

B. Dynamics

In this section, we present calorimetric and dielectric spectroscopy results for all investigated nanocomposites and pure PMMA. The aim here is not a comprehensive study of the glass transition related dynamics of PMMA but merely the identification of the major characteristics of the dynamics, with particular attention on the effect of silica particles on such dynamics.

Fig. 2 shows the DSC scans for pure PMMA and the three investigated nanocomposites, obtained at 10 °C.min^{-1}, on cooling. For all samples, a step in the heat capacity, corresponding to the glass transition of PMMA, is clearly observed. With the addition of silica, neither the shape nor the position of the glass transition are affected.

Fig. 3 shows the dielectric loss ε'' of pure PMMA versus the logarithm of the frequency at different temperatures. A single ε'' peak is observed at temperatures both above and below T_g. The frequency of the maximum, f_{max}, of these spectra shifts to higher frequencies with increasing temperature. This result indicates enhanced molecular mobility with increasing temperature. The dielectric response of pure PMMA (Fig. 3) is in good agreement with previous studies reported in the literature.[57–61] The relaxational process below T_g has been reported to be associated with a PMMA β-process.[51,62] On the other hand, at temperatures higher than T_g, the dielectric response of PMMA has been shown to be the superposition of the α-process, associated with the glass transition, and the β-process. In the case of the methacrylate polymers, it has been shown that the β-process dominates the dielectric response.[51,62]

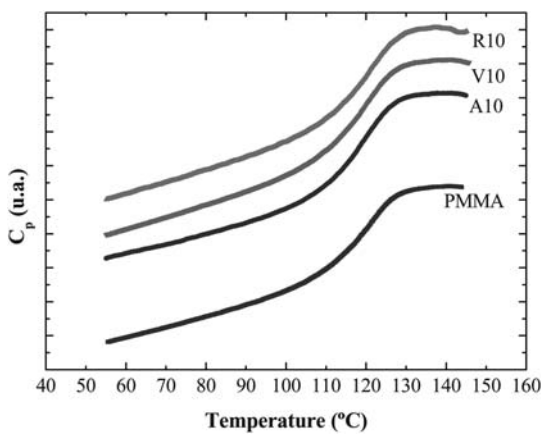

Fig. 2 Temperature variation of the specific heat capacity of PMMA and nanocomposites normalized to the amount of PMMA.

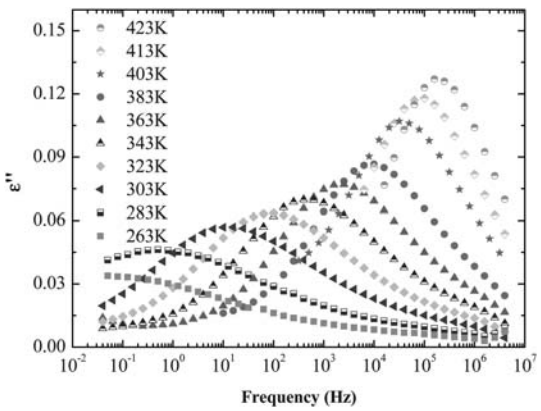

Fig. 3 Dielectric loss of pure PMMA versus frequency, at different temperatures ranging from 263 K to 423 K.

Fig. 4 compares the normalized dielectric loss versus frequency of PMMA and the three nanocomposites. Such curves are presented at three different temperatures: 353 K, 393 K and 423 K, representative respectively of the dielectric response below, around, and above T_g. Whatever the temperature range, any difference in the shape, the width, or the relaxation time can hardly be observed in the dielectric loss versus frequency curves. This result is clearly illustrated in Fig. 5, where the decimal logarithm of the relaxation time corresponding to the frequency of the maximum of dielectric loss *vs.* frequency spectra, is plotted as a function of the inverse of the temperature. In this figure, it is evident that PMMA segmental mobility is not affected by the presence of silica. This similarity between the dynamics of nanocomposites and pure PMMA is in accordance with the DSC results showing no difference in T_g.

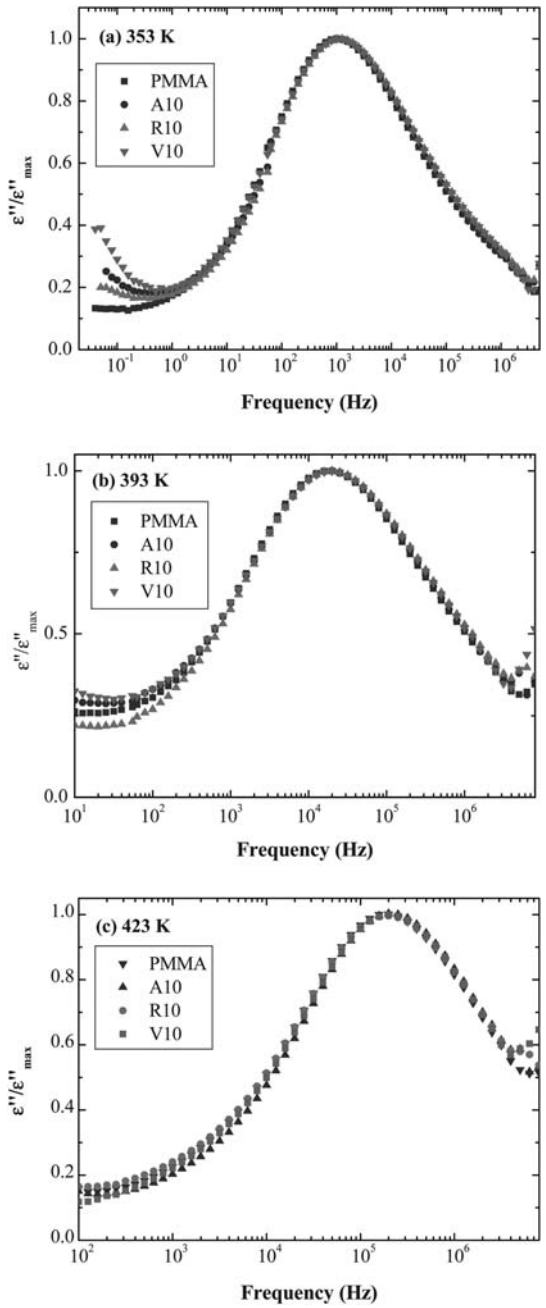

Fig. 4 Normalized dielectric loss versus frequency curves of PMMA and the three nanocomposites, at: a) $T < T_g$ (353 K), b) $T \sim T_g$ (393 K), and c) $T > T_g$ (423 K).

C. Physical aging study monitored by broadband dielectric spectroscopy

As already pointed out in the Introduction, physical aging corresponds to the thermodynamically driven time evolution of the structure towards the equilibrium state, resulting in the modification of the glass physical properties with time. As far as dielectric properties are concerned, during the course of physical aging the dielectric permittivity can show two opposing trends:[39] (i) it increases due to the increased number of polarizable entities per unit volume; or (ii) in the case of orientation polarization due to relaxed molecular dipoles, the permittivity decreases due to a reduced amplitude of angular fluctuations, which usually establish the secondary relaxation processes in the glassy state. This latter effect was shown in the past to be dominant during physical aging of amorphous poly(ethylene terephthalate) (PET) and related polyesters,[63] in polycarbonate[27,39] and in poly(vinyl ethylene) (PVE),[64] whereas the former effect has been found during PS physical aging.[65]

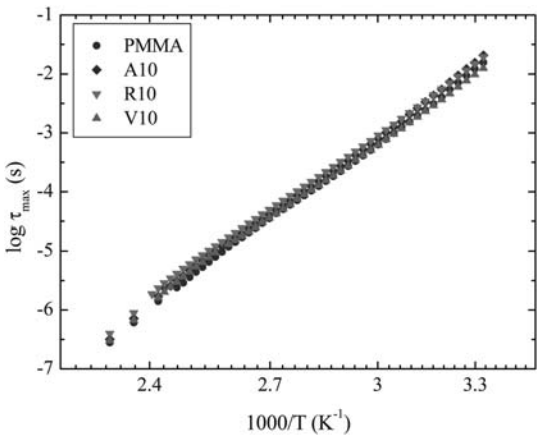

Fig. 5 Temperature dependence of the decimal logarithm of relaxation time, for pure PMMA and PMMA/silica nanocomposites.

In the present study, the latter trend was found for PMMA and therefore, during aging, the β-relaxation decreases in amplitude as a consequence of the densification of the system. This is shown in Fig. 6, where the normalized dielectric loss, namely, the ratio of the actual loss with the maximum of the loss at the initial aging time, is plotted versus frequency, at 353 K as an example, for pure PMMA and the nanocomposite V10. The so-defined normalized dielectric permittivity is shown at the following aging times: the initial aging time, corresponding to the inherent experimental delay time (t_d) of 10^3 s needed to stabilize the sample at the selected aging temperature (black squares for PMMA and light grey triangles for V10); and

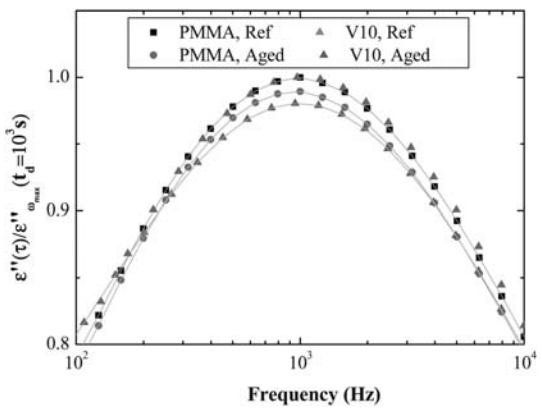

Fig. 6 Comparison of the normalized dielectric losses of PMMA and V10 versus frequency at the initial aging time t_d of 10^3 s (black squares for PMMA, light grey triangles for V10), and after an aging time t_a of 1,1x10^4 s (circles for PMMA, dark grey triangles for V10), at T_a = 353 K. Continuous lines are the fits through the HN-functions.

1.1×10^4 s aging time (dark grey triangles for V10 and circles for PMMA). The decrease of the normalized dielectric permittivity is clearly larger for the nanocomposite V10. Thus, according to these first observations, the physical aging process seems to be faster in the nanocomposite V10. A similar result was found for the nanocomposites A10 and R10 (not shown), which also displayed accelerated physical aging in comparison to pure PMMA. As will be seen later in the paper, the latter nanocomposites exhibit similar aging rates. Furthermore, the physical aging process is, in both A10 and R10 and at all temperatures, slower than in the nanocomposite V10.

As has already been mentioned in the Experimental section, the reduction of ε'' results in a decrease in the relaxation strength ($\Delta\varepsilon$) of the β process. This magnitude can be used to define a relaxation function, which is required to quantitatively analyze physical aging data. In the past, the following relaxation function was defined to describe the volume and enthalpy relaxation of glasses:[66,67]

$$\phi(t) = \frac{X(t) - X(\infty)}{X(0) - X(\infty)} \quad (4)$$

where $X(t)$, $X(\infty)$, $X(0)$ are respectively the values of the volume or the enthalpy at aging time t, at equilibrium and at zero aging time.

The so-defined relaxation function is an appropriate mathematical tool to quantitatively study physical aging, since it takes into account the thermodynamic driving force for aging. This is actually defined by the quantity $X(0) - X(\infty)$. Thus the relaxation function $\phi(t)$ allows a non-ambiguous definition of the physical aging rate for those systems displaying different thermodynamic driving forces or for the same system at different aging temperatures. This concept is schematically sketched in the inset of Fig. 7a, where we present the temperature dependence of a typical thermodynamic property of a glass-forming system. Thus the aging rate is a result of the competition between the thermodynamic driving force for aging, which is larger at temperatures well below T_g, and mobility, which increases with temperature.[68]

In analogy to thermodynamic functions, the structural relaxation function $\phi(t)$ associated with the dielectric relaxation strength was evaluated using the following relation:

$$\phi(t) = \frac{\Delta\varepsilon(t) - \Delta\varepsilon(\infty)}{\Delta\varepsilon(0) - \Delta\varepsilon(\infty)} \quad (5)$$

where $\Delta\varepsilon(t)$ is the dielectric strength value at any aging time t, $\Delta\varepsilon(\infty)$ is the equilibrium dielectric strength value, and $\Delta\varepsilon(0)$ is the dielectric strength value prior to aging.

The use of this relaxation function to define the physical aging rate can be justified by the fact that the temperature dependence of the dielectric strength $\Delta\varepsilon$ mimics the variation of the thermodynamic functions (H, V, *etc.*). The correspondence between the dielectric strength of the secondary relaxation and thermodynamic properties has been already demonstrated by Power *et al.*[69] presenting dielectric relaxation data for glass-forming D-sorbitol. In our study, this correspondence is well illustrated in Fig. 7a, where the dielectric strength of the PMMA β process is displayed as a function of temperature. In this figure, the extrapolations of the glassy line and of the equilibrium line

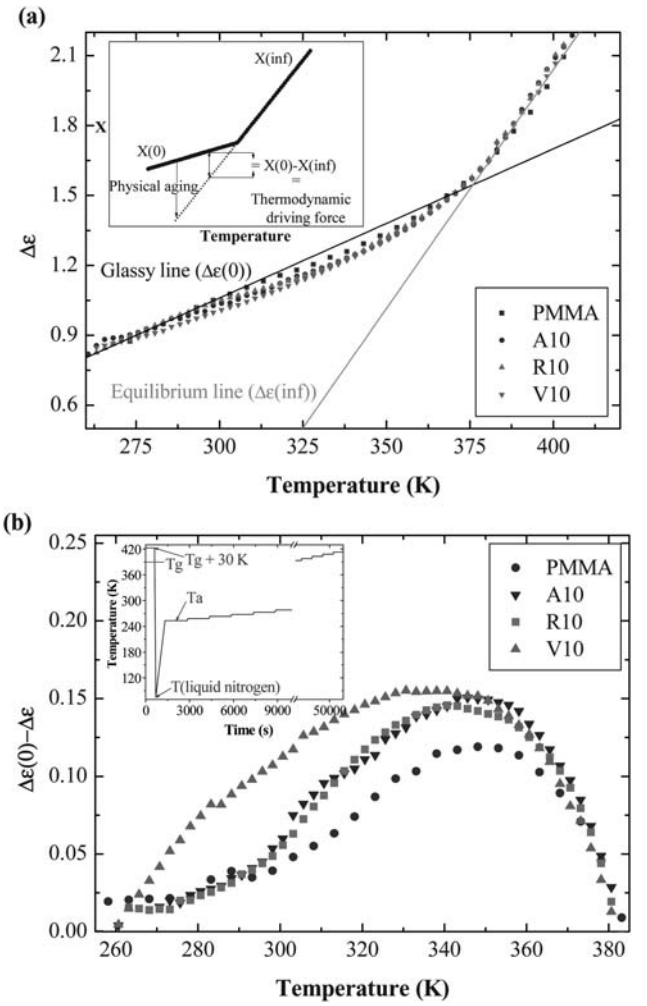

Fig. 7 (a) Temperature dependence of the β-dielectric relaxation strength. The continuous lines result from the extrapolations of the PMMA glassy line from 260 K, and of the equilibrium line above T_g. The inset of (a) illustrates the temperature dependence of a typical thermodynamic property of a glass-forming system, and proposes a schematic definition of the thermodynamic driving force for physical aging. (b) $\Delta\varepsilon(T)$ deviation from the glassy line, referred to as $\Delta\varepsilon(0) - \Delta\varepsilon$. The inset of (b) sketches the temperature program applied to obtain the curves plotted in (b).

provide the values of respectively $\Delta\varepsilon(0)$ and $\Delta\varepsilon(\infty)$ at any temperature.

It is worth noticing that the temperature dependence of $\Delta\varepsilon$ shows that the glassy lines obtained from the different samples collapse for temperatures lower than that at which $\Delta\varepsilon(T)$ starts to show a down-shift from the glassy line (see Fig. 7a). This shift of $\Delta\varepsilon(T)$ from the glassy line is directly linked to the physical aging occurring during the dielectric measurement. Indeed, as shown in the inset to Fig. 7b, a time of about 10 min elapses during each isothermal frequency scan. During this time, provided that the temperature is high enough to have significant aging effects, the value of $\Delta\varepsilon(T)$ deviates from that of the glassy line. Therefore, the increased $\Delta\varepsilon(T)$ shift from the glassy line with temperature is the result of the accumulated physical aging occurred during each isothermal frequency scan. Fig. 7a also shows that the equilibrium lines obtained from all samples collapse above the

glass transition temperature T_g. This observation is consistent with the fact that all samples present the same equilibrium dynamics, as shown by DSC and BDS results.

In Fig. 7b, the difference between $\Delta\varepsilon(0)$ and the observed $\Delta\varepsilon$ is presented as a function of temperature. This plot highlights the fact that physical aging is faster in nanocomposites. Indeed, not only is the deviation value more important in the nanocomposites but it is also observed at lower temperatures. Furthermore, such deviation is more pronounced for the nanocomposite V10 in comparison to the other nanocomposites (A10 and R10).

These results are consistent with the acceleration of physical aging observed in isothermal plots of the dielectric loss of the dielectric permittivity versus frequency at different aging times (see Fig. 6).

Fig. 8 shows as an example the relaxation function $\phi(t)$ normalized to $\phi(t_d)$ for the nanocomposite V10, as a function of the aging time and for different aging temperatures. From the inspection of the figure, it is evident that the evolution towards equilibrium is faster at higher temperatures. Moreover, the relaxation function of the dielectric strength can be approximately described as a linear function of the logarithmic aging time, at least in the observation time window. This result is in agreement with previous structural relaxation studies using volumetric,[70] dynamic mechanical spectroscopy, creep and positron data.[71]

An interesting study is the comparison of $\phi(t)/\phi(t_d)$ for all samples, at a fixed temperature, as shown in Fig. 9. Whatever the aging temperature T_a value, in the range 303 K–353 K, the same tendency is observed. The so-called physical aging rate,[70] which corresponds to the slope of $\phi(t)/\phi(t_d)$ versus aging time, is higher for the nanocomposite samples relative to the pure polymer. In particular, the physical aging is faster for the nanocomposite V10 in comparison to A10 and R10, which display equivalent aging rates. The accelerated physical aging observed for the nanocomposites in comparison to pure PMMA is in agreement with the results presented in Fig. 6.

The similarity of the aging rates of the nanocomposites A10 and R10 implies on one hand that the physical aging is independent of the surface treatment of the silica particles, at least for the samples investigated in this work. On the other hand, these results provide an indication that the physical aging rate depends on the silica particles size and, therefore, on the silica surface/volume of PMMA ratio. In other words, for the investigated nanocomposite samples, a higher silica surface/volume of PMMA ratio is found to be associated with a faster physical aging process.

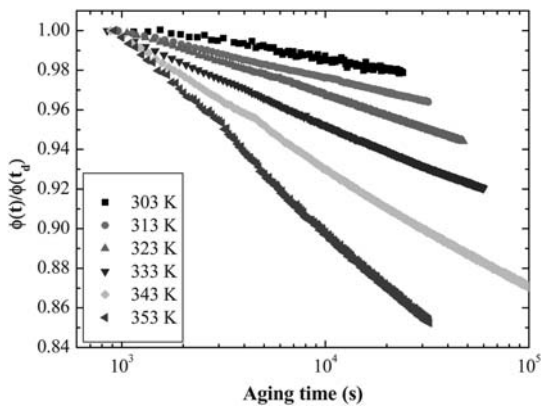

Fig. 8 Normalized dielectric relaxation function $\phi(t)/\phi(t_d)$ of the sample V10 versus aging time, at different temperatures, ranging from 303 K to 353 K. See text for the definition of normalized dielectric relaxation function.

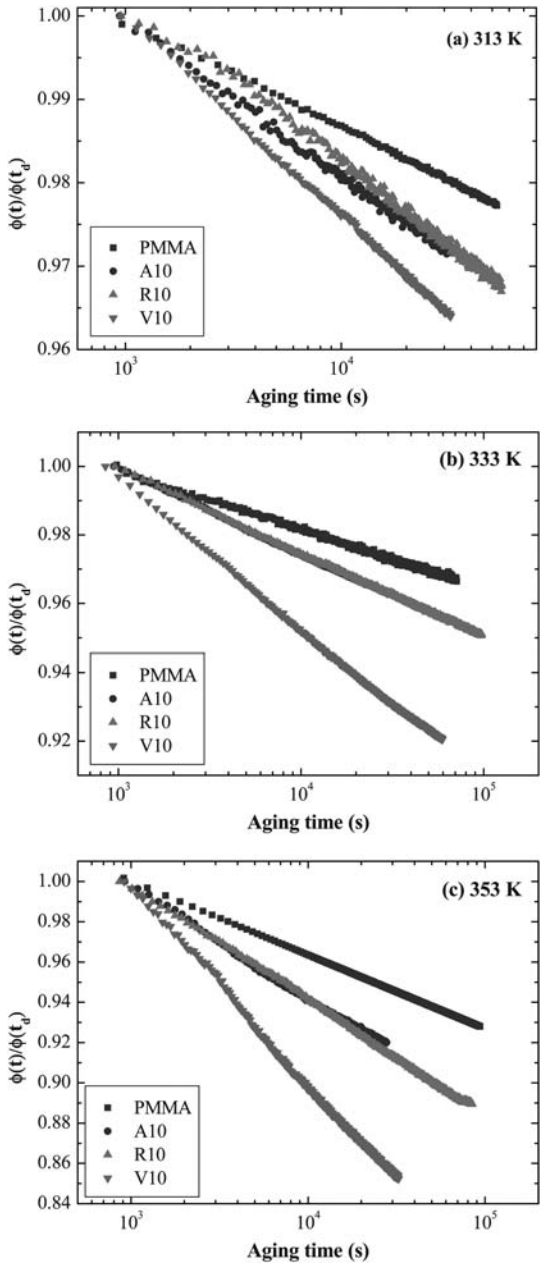

Fig. 9 Comparison of the normalized dielectric relaxation functions. $\phi(t)/\phi(t_d)$ obtained for PMMA and the nanocomposites versus aging time, at different temperatures: a) 313 K; b) 333 K, c) 353 K. See text for the definition of normalized dielectric relaxation function.

IV. Application of the diffusion model

Although physical aging in bulk polymers has been the subject of a large number of studies since the pioneering works of Simon,[72]

Kovacs[6] and Struik,[5] the study of such a phenomenon in confined polymers is still in its early stages.[17–33] Nevertheless, one can observe that the major part of the studies on materials confined to the nanometre scale highlights the reduction, or even the suppression, of physical aging.[19,20,34] On the other hand, it has been shown that polymers confined to the micrometre scale present enhanced physical aging.[24,27,30,35–39]

The modification of physical aging rate is most of the time attributed to the modification of the polymer dynamics, shown by a shift in the glass transition temperature.[14–18] However, some effects of confinement on aging cannot be explained by changes in T_g. While reductions in physical aging with confinement have been attributed to interfacial effects perturbing molecular mobility,[19–26] enhancements in physical aging with confinement have been explained by models[27,46] based on free volume loss during structural relaxation.[73]

Within the framework of our study, one can hardly invoke a modification in the polymer dynamics to explain the observed acceleration of physical aging in PMMA/silica nanocomposites, considering that the dynamics remains unchanged in the presence of silica particles. As a necessary consequence, another explanation for the modification of physical aging rates in polymer nanocomposites needs to be established. This explanation must lie in the comprehension of the underlying mechanism of physical aging.

As mentioned in the Introduction section, a possible explanation for the accelerated physical aging in PMMA/silica nanocomposites may be sought in the diffusion of free volume holes and their disappearance at a boundary surface, which, in this case, is represented by the polymer/particle interface. Thus our data were analyzed according to the diffusion model. Within this framework, the diffusion of free volume can be expressed by the second equation of Fick:

$$\frac{\partial f_v}{\partial t} = \nabla(D\nabla f_v) \tag{6}$$

where f_v is the free volume fraction and D is the diffusion coefficient. If we expand eqn (6) for short times, we can assume a constant D, since the well-known effect of self-retardation[5] has not yet provoked a substantial decrease of D. Within this simplified picture, the total number of free volume holes at time t, $N(t)$, equals the integral over the sample volume of the free volume. Rearranging eqn (6), the following expression for $N(t)$ can be obtained for short aging times:

$$\frac{N(t)}{N(0)} = 1 - \frac{2}{\pi^{0.5}}\frac{A}{V}D^{0.5}t^{0.5} \tag{7}$$

where A is the total surface where free volume holes disappear, V is the total volume, D is the diffusion coefficient at zero aging time, t is the aging time, and $N(0)$ is the number of holes at the initial aging time.

This equation can be applied to our structural relaxation function $\phi(t)$, if we make the reasonable assumption that the variation of the free volume produces a linearly proportional variation in the dielectric relaxation strength, at least in the vicinity of $t = 0$. Therefore, eqn (7) can be written in terms of the dielectrically defined relaxation function $\phi(t)$.

$$\phi(t) = 1 - \frac{2}{\pi^{0.5}}\frac{A}{V}D^{0.5}t^{0.5} \tag{8}$$

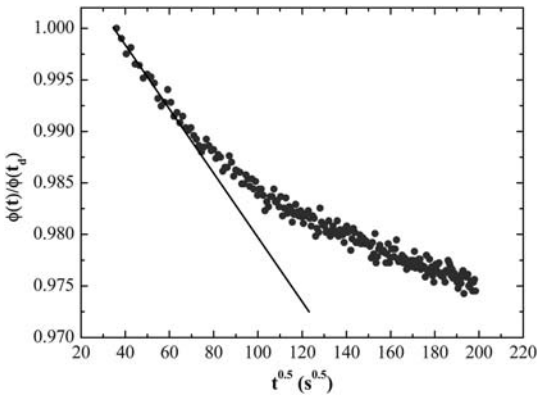

Fig. 10 Derivative of the normalized relaxation function $\phi(t)/\phi(t_d)$ with the square root of the aging time for pure PMMA at 333K. The continuous line represents the tangent to the curve at zero aging time.

Eqn (8) can be differentiated with respect to the square root of the time at $t = 0$:

$$\left.\frac{\partial\phi(t)}{\partial t^{0.5}}\right|_{t\approx 0} = -\frac{2}{\pi^{0.5}}\frac{A}{V}D^{0.5} \tag{9}$$

to obtain information on the diffusion coefficient at the beginning of the aging process. This can be obtained from the slope of the tangent to $\phi(t)$ versus $t^{0.5}$ plots at the initial stages of the aging process, once the area to volume ratio (A/V) is known, as illustrated in Fig. 10. In the case of PMMA/silica nanocomposites, this ratio corresponds to the amount of the PMMA/silica interface divided by the volume of PMMA. For pure PMMA, as a first attempt, the area to volume ratio was identified with the inverse of the macroscopic dimensions of the sample (around 200 μm). The ratios A/V considered for the determination of diffusion coefficients are reported in Table 2.

The diffusion coefficients obtained for all samples were then plotted versus the inverse of the temperature. This is reported in Fig. 11, where it is evident that diffusion coefficients of all nanocomposite samples approximately collapse to the same values at each temperature. This result is in agreement with the hypothesis of the diffusion mechanism for physical aging, considering that the diffusion coefficient must be only dependent on the mobility of PMMA in the nanocomposites, which has been shown to be unaffected by the presence of silica particles.

Moreover, the temperature dependence of the diffusion coefficient can be well described by the Arrhenius law: $D = D_0\exp(-E_a/kT)$, where k is the Boltzmann constant and D_0 is the pre-exponential factor, with an activation energy of $E_a = 65 \pm 13$ kJ mol^{-1}. Interestingly, this value of the activation energy is comparable to the one of the PMMA

Table 2 Summary of calculated and experimental parameters from permittivity measurements for the nanocomposites samples

Sample	Theoretical interparticle distance, l (nm)	Area to volume ratio, A/V (nm^{-1})	Diffusion coefficient, D, at 333 K (cm^{-1})
A10	1410	8.0×10^{-4}	1.05×10^{-14}
R10	1410	8.0×10^{-4}	6.90×10^{-15}
V10	806	1.4×10^{-3}	6.83×10^{-15}

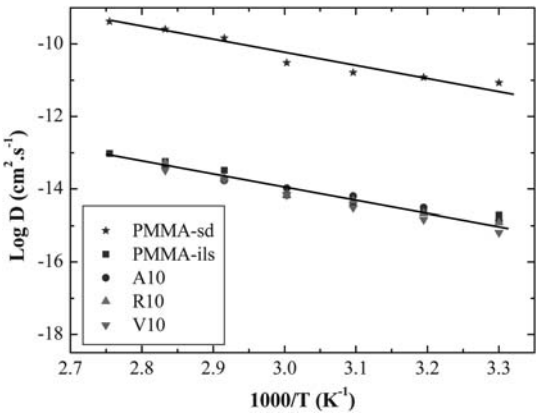

Fig. 11 Decimal logarithm of the diffusion coefficient, as a function of the inverse of temperature, for the nanocomposites and for pure PMMA: "PMMA-sd" refers to the values obtained introducing the sample dimensions in eqn (9); "PMMA-ils" corresponds to the values obtained introducing an internal length scale for diffusion in eqn (9). The continuous lines are the fits through the Arrhenius law.

β-process (80 ± 3 kJ mol^{-1}), determined from the plot of the relaxation time as a function of the inverse temperature reported in Fig. 5. This result is in agreement with previous works on physical aging of both polymeric[5,74] and non-polymeric[75–77] glass formers in which it was also concluded that the activation energy of the physical aging process is of the same order of magnitude as the one of the secondary relaxation process.

Concerning the apparent diffusion coefficient of pure PMMA, one can observe that the values obtained inserting the macroscopic dimensions of the sample in eqn (9) are unphysically large (star symbols in Fig. 11). However, the diffusion activation energy of the PMMA sample is the same as that of nanocomposites, namely comparable to that of the PMMA β-process. This discrepancy between apparent diffusion coefficients for PMMA and nanocomposite samples could be explained according to two different hypotheses.

The first hypothesis is that the physical aging in bulk glasses, resulting in a reduction of the free volume, predominantly occurs *via* lattice contraction, as proposed by McCaig *et al.*[37,38] to describe physical aging in glassy polyarylate. In this case, due to the large dimensions of the sample, the diffusion mechanism would produce negligible effects on the free volume reduction.

The second hypothesis is based on the existence of an internal length scale for diffusion of free volume holes in PMMA, as proposed by Curro *et al.*[73] and Cangialosi *et al.*[27,39] to explain the sample thickness independence of physical aging rates in respectively poly(vinyl acetate) (PVAc) and polycarbonate (PC). According to Cangialosi *et al.*,[27,39] this internal length scale is somehow created during cooling from the supercooled state. In particular, it is assumed that the inhomogeneity of the glass gives rise to low-density regions that act as an internal surface for vacancy annihilation. Thus the internal length scale for diffusion of free volume holes corresponds to the average distance between these low-density regions. This latter approach was applied for the determination of the adequate ratio A_{int}/V for PMMA to obtain comparable diffusion coefficients for PMMA and nanocomposites at zero aging time, as shown in Fig. 11 (square symbols).

The so-obtained value of A_{int}/V, allowed the determination of the value of the internal length scale for diffusion of free volume holes in PMMA. The internal length scale for diffusion of free volume in PMMA was found to be around 3 μm, which is of the same order of magnitude of those obtained by Curro *et al.*[73] for PVAc and Cangialosi *et al.*[27,39] for PC.

V. Discussion

In the previous section of the paper, we have applied the idea of the diffusion mechanism to explain the apparently contradictory result of accelerated physical aging in PMMA/silica nanocomposites, in which the polymer segmental dynamics is invariant in comparison to bulk PMMA. Within the diffusion mechanism framework, we have emphasized the crucial role of the ratio between the surface of particles and the volume of polymer in affecting the physical aging process in polymer nanocomposites. The relatively large value of such a ratio is, according to eqn (9), responsible for the observed acceleration of physical aging. Thus we provide a direct link with the physical aging of thin polymer films with thickness in the micrometre range, where the area to volume ratio of the sample is also relatively large in comparison to the corresponding bulk material. The physical aging of the latter systems has also been successfully described hypothesizing the diffusion of free volume holes towards the external surface.[27,37,38,39] However, in these studies no information about the mobility of the investigated systems was presented. Thus, our study provides clear indications that the enhanced rate of physical aging does not bear *any* relation with a change of the molecular mobility associated with the glass transition of the polymer. This statement contradicts a recent conclusion drawn by Rowe *et al.*,[50] who reported the profile of free volume characteristics by means of a variable energy positron annihilation spectroscopy study during physical aging of thin films of polysulfone (PSF). They found a reduction in the free volume size but not in their number and, thus, ruled out the possibility of diffusion of free volume holes towards the external surface, which would actually result in a decrease in their number. Thus, the more pronounced reduction of the free volume size at the external surface was explained by an enhanced segmental mobility in the region of 50–100 nanometres from the surface. However, such an interpretation contrasts with simulation studies by Scheidler *et al.*,[43] who showed that the mobility near a surface is affected only in the first 1–2 nanometres from the surface. This interpretation is also in disagreement with experimental observations by solvation dynamics[44] and nuclear magnetic resonance[45] in low molecular weight glass formers confined in nanopores, which provide evidence that the molecular mobility of the bulk system is restored at distances not larger than 4 nm from the external surface. Furthermore, recent BDS experiments on ultra-thin polymer films do not provide an indication of a change in segmental dynamics in comparison to bulk polymers at thicknesses as small as 10 nm.[78–80]

So far we have tackled our hypothesis of the diffusion of free volume holes considering physical aging results on systems with a typical length scale larger than few hundred nanometres. However, it is also worth discussing recent physical aging studies in nanostructured materials with typical size shorter than 100 nm, in the light of the diffusion mechanism. PMMA/silica

nanocomposite physical aging has been investigated by Priestley *et al.*[21] employing fluorescence spectroscopy. They investigated systems with 0.4% vol. of 10–15 nm silica nanoparticles and concluded that physical aging at 296 K is suppressed. This result is, at least apparently, at odds with ours. However, it has to be remarked that in ref. 21 the amount of interface to volume of PMMA ratio (associated to the interparticle distance) is considerably larger than in the case of our systems. This means that, within the diffusion mechanism, such a large area to volume ratio would lead to a strongly enhanced physical aging rate. Thus, a possible interpretation of the result of Priestley *et al.*[21] would be that the physical aging process occurs in a time scale shorter than the delay time (inherent to any experimental technique) required to reach the selected aging temperature.

A similar explanation could be given to interpret the apparent reduction, or even suppression, of physical aging in other nanostructured systems. In particular, physical aging has been found to be strongly reduced at the free surface of thin films of PMMA.[20] Analogous results were found by Kawana and Jones when monitoring physical aging of thin films of PMMA[34] and by Fukao and Koizumi investigating this process in PS thin films.[65] A notable exception is represented by the work of Simon *et al.*,[18] who observed accelerated physical aging in OTP confined in nanopores in comparison to the bulk system. As far as the studies reporting a reduction or suppression of physical aging at the scale of nanometres are concerned, such a reduction or suppression could also be explained assuming that the glass has already reached (or almost reached) the equilibrium when collecting the first data during a physical aging experiment. This occurrence is schematically sketched in Fig. 12, where typical relaxation functions are displayed versus the aging time. As can be observed, two possibilities for explaining the lack of time evolution of the relaxation functions can be put forward: i) physical aging is slow enough to be absent in the available time window, which depends on the temperature stabilization time and on the selected maximum aging time (right line in Fig. 12); ii) physical aging has already occurred before the first experimental data can be acquired (left line in Fig. 12). On one hand, the occurrence of the latter scenario would be compatible with the idea of diffusion driven accelerated physical aging, also in nanostructured systems with typical confinement length shorter than about 100 nm. The latter scenario is also in agreement with recent results by Rowe *et al.*[81] who measured the evolution of gas permeability in several glassy polymers. They showed that, although for ultra-thin polymer films (less than 50 nm) the time evolution of the permeability is dumped in comparison to the thickest films, the initial value of this property is consistently reduced with respect to the "bulk" value. In light of these results, the idea that the physical aging is already consistently advanced when the first permeability data are recorded is a plausible scenario. On the other hand, the former scenario (i) can be an alternative interpretation for the suppression of physical aging in PMMA/silica and P2VP/silica nanocomposites reported by Rittigstein *et al.*,[21,22] and explained by strong hydrogen bonding between silica particles and each of the two polymers. This possibility can not, at the present time, be discarded. However, this interpretation would not be completely convincing to interpret the absence of physical aging in PS 10 nm thin films,[34] where the presence of hydrogen bonds with the substrate can not be invoked.

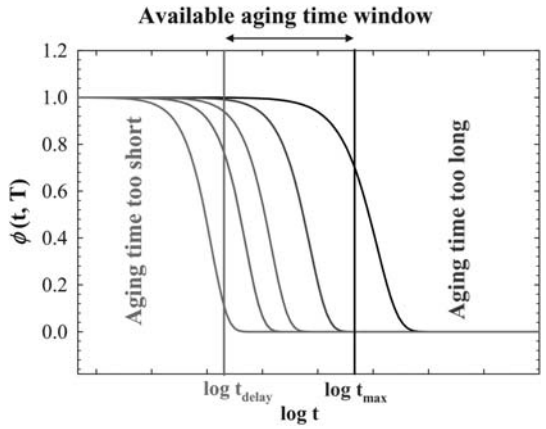

Fig. 12 Typical variation of different relaxation functions $\phi(t)$ with the logarithm of the aging time and schematic representation of the experimental available aging time window. The time t_{delay} corresponds to the inherent delay time needed to reach the selected aging temperature; the time t_{max} corresponds to the maximum time employed in conventional physical aging experiments.

VI. Summary and conclusions

We have characterized PMMA/silica nanocomposites in terms of nanoparticle dispersion and dynamics. This preliminary characterization has shown a very good dispersion of silica nanoparticles in PMMA, whatever the silica surface treatment chemical nature, and whatever the silica nanoparticle dimensions. It has also been shown that the incorporation of silica nanoparticles in bulk PMMA has no influence on PMMA dynamics as measured by DSC and BDS.

We have also studied the physical aging of PMMA and PMMA/silica nanocomposites in the temperature range 273–353 K by monitoring the time evolution of PMMA secondary relaxation strength. The effect of the presence of silica nanoparticles in PMMA was investigated, as well as the effect of silica nanoparticle dimensions and silica nanoparticle surface treatment chemical nature. The dielectric strength associated with the β-process was found to decrease during physical aging, due to the decreased orientational polarization as a consequence of densification. Dielectric relaxation strength data were described by a normalized relaxation function which allowed the comparison among the samples. It was found that the physical aging process is not only faster in the presence of silica nanoparticles, but it also seems to be dependent on silica nanoparticle dimensions, or rather silica surface/volume of PMMA ratio, a higher silica surface/volume of PMMA ratio giving rise to a faster physical aging process.

Dielectric relaxation strength data were fitted according to a diffusion model. The outcome was that this diffusion model accurately describes the experimental results, and in particular the tendency of physical aging rate to depend on the silica surface/volume of PMMA ratio in nanocomposites. Furthermore, a strong similarity between the activation energy of the diffusion coefficient of free volume holes and that of the PMMA β-process was found, suggesting that the latter process is responsible for the diffusion of free volume holes. The good description of the time dependence of dielectric relaxation strength by means of a diffusion model suggests that physical

aging in polymer nanocomposites is driven by the diffusion of free volume holes to the interfaces between the polymer and nanoparticles.

Acknowledgements

The authors acknowledge the University of the Basque Country and Basque Country Government (Ref. No. IT-436-07, Depto. Educación, Universidades e Investigación) and Spanish Minister of Education (Grant No. MAT 2007-63681) for their support. The support of the European Community within the SOFT-COMP program is also acknowledged. The SGIker UPV/EHU is gratefully acknowledged for the electron microscopy facilities of the Guipuzkoa unit.

References

1 F. Hussain, M. Hojjati, M. Okamoto and R. Gorga, *J. Compos. Mater.*, 2006, **40**, 1511–1575.
2 D. Blond, V. Barron, M. Ruether, K. Ryan, V. Nicolosi, W. Blau and J. Coleman, *Adv. Funct. Mater.*, 2006, **16**, 1608–1614.
3 J. Coleman, M. Cadeck, K. Ryan, A. Fonseca, J. Nagy, W. Blau and M. Ferreira, *Polymer*, 2006, **47**, 8556–8561.
4 B. Ash, R. Siegel and L. Schadler, *Macromolecules*, 2004, **37**, 1358–1369.
5 L. C. E. Struik, in *Physical aging in amorphous polymers and other materials*, Elsevier, Amsterdam, 1978.
6 A. J. Kovacs, J. J. Aklonis, J. M. Hutchinson and A. R. Ramos, *J. Polym. Sci. Polym. Phys.*, 1979, 1097–1162.
7 Here and throughout the manuscript, we refer to "molecular mobility" as the local dynamics of the glass (α and β processes). Thus, larger scale dynamics (Rouse, Reptation *etc.*) are excluded from our discussion.
8 R. D. Priestley, *Soft Matter*, 2009, **5**, 919–926.
9 G. Adam and J. H. Gibbs, *J. Chem. Phys.*, 1965, **43**, 139–146.
10 K. L. Ngai, *J. Phys. IV*, 2000, **10**, 7–21.
11 T. A. Tran, S. Saïd and Y. Grohens, *Composites, Part A*, 2005, **36**, 461–465.
12 J. L. Keddie, R. A. L. Jones and R. A. Cory, *Europhys. Lett.*, 1994, **27**, 59–64.
13 J. A. Forrest, K. Dalnoki-Veress, J. R. Stevens and J. R. Dutcher, *Phys. Rev. Lett.*, 1996, **77**, 2002–2005.
14 C. J. Ellison and J. M. Torkelson, *Nat. Mater.*, 2003, **2**, 695–700.
15 D. S. Fryer, R. D. Peters, E. J. Kim, J. E. Tomaszewski, J. J. de Pablo and P. F. Nealey, *Macromolecules*, 2001, **34**, 5627–5634.
16 C. H. Park, J. H. Kim, M. Ree, B.-H. Sohn, J. C. Jung and W.-C. Zin, *Polymer*, 2004, **45**, 4507–4513.
17 Y. Huang and D. R. Paul, *Polymer*, 2004, **45**, 8377–8393.
18 S. L. Simon, J. Y. Park and G. B. McKenna, *Eur. Phys. J. E*, 2002, **8**, 209–216.
19 R. D. Priestley, L. J. Broadbelt and J. M. Torkelson, *Macromolecules*, 2005, **38**, 654–657.
20 R. D. Priestley, C. J. Ellison, L. J. Broadbelt and J. M. Torkelson, *Science*, 2005, **309**, 456–459.
21 R. D. Priestley, P. Rittigstein, L. J. Broadbelt, K. Fukao and J. M. Torkelson, *J. Phys.: Condens. Matter*, 2007, **19**, 205120.
22 P. Rittigstein and J. M. Torkelson, *J. Polym. Sci., Part B: Polym. Phys.*, 2006, **44**, 2935–2943.
23 D. P. N. Vlasveld, H. E. N. Bersee and S. J. Picken, *Polymer*, 2005, **46**, 12539–12545.
24 Y. Huang and D. R. Paul, *Macromolecules*, 2006, **39**, 1554–1559.
25 K. Fukao and A. Sakamoto, *Phys. Rev. E: Stat., Nonlinear, Soft Matter Phys.*, 2005, **71**, 041803.
26 H. Lu and S. Nutt, *Macromolecules*, 2003, **36**, 4010–4016.
27 D. Cangialosi, M. Wubbenhorst, J. Groenewold, E. Mendes and S. J. Picken, *J. Non-Cryst. Solids*, 2005, **351**, 2605–2610.
28 H. Richardson, C. Carelli, M. Sferrazza and J. L. Keddie, *Eur. Phys. J. E*, 2003, **12**, 437–441.
29 H. Richardson, I. Lopez-Garcia, M. Sferrazza and J. L. Keddie, *Phys. Rev. E: Stat., Nonlinear, Soft Matter Phys.*, 2004, **70**, 051805.
30 K. Dorkenoo and P. H. Pfromm, *Macromolecules*, 2000, **33**, 3747–3751.
31 C. C. Wong, Z. Qin and Z. Yang, *Eur. Phys. J. E*, 2008, **25**, 291–298.
32 D. Punsalan and W. J. Koros, *Polymer*, 2005, **46**, 10214–10220.
33 C. Zhou, T. S. Chung, R. Wang and S. H. Goh, *J. Appl. Polym. Sci.*, 2004, **92**, 1758–1764.
34 S. Kawana and R. A. L. Jones, *Eur. Phys. J. E*, 2003, **10**, 223–230.
35 P. H. Pfromm and W. J. Koros, *Polymer*, 1995, **36**, 2379–2387.
36 K. D. Dorkenoo and P. H. Pfromm, *J. Polym. Sci., Part B: Polym. Phys.*, 1999, **37**, 2239–2251.
37 M. S. McCaig and D. R. Paul, *Polymer*, 2000, **41**, 629–637.
38 M. S. McCaig, D. R. Paul and J. W. Barlow, *Polymer*, 2000, **41**, 639–648.
39 D. Cangialosi, M. Wübbenhorst, J. Groenewold, E. Mendes, H. Schut, A. van Veen and S. J. Picken, *Phys. Rev. B: Condens. Matter Mater. Phys.*, 2004, **70**, 224213.
40 E. Donth, E. Hempel and C. J. Schick, *J. Phys.: Condens. Matter*, 2000, **12**, L281–L286.
41 D. Cangialosi, A. Alegría and J. Colmenero, *Phys. Rev. E: Stat., Nonlinear, Soft Matter Phys.*, 2007, **76**, 011514.
42 S. Karmakara, C. Dasguptaa and S. Sastryb, *Proc. Natl. Acad. Sci. U. S. A.*, 2009, **106**(10), 3675–3679.
43 P. Scheidler, W. Kob and K. Binder, *Europhys. Lett.*, 2002, **59**, 701–707.
44 F. He, L. M. Wang and R. Richert, *Phys. Rev. B: Condens. Matter Mater. Phys.*, 2005, **71**, 144205.
45 S. Gradmann, P. Medick and E. A. Rossler, *J. Phys. Chem. B*, 2009, **113**, 8443–8445.
46 T. Alfrey, G. Goldfinger and H. Mark, *J. Appl. Phys.*, 1943, **14**, 700–705.
47 G. Braun and A. J. Kovacs, *Phys. Chem. Glasses*, 1963, **4**, 152–160.
48 J. G. Curro, R. R. Lagasse and R. Simha, *Macromolecules*, 1982, **15**, 1621–1626.
49 J. Perez, *Polymer*, 1988, **29**, 483–489.
50 B. W. Rowe, B. D. Freeman and D. R. Paul, *Polymer*, 2009, **50**, 6149–6156.
51 R. Bergman, F. Alvarez, A. Alegría and J. Colmenero, *J. Chem. Phys.*, 1998, **109**, 7546–7555.
52 G. H. Bogush, M. A. Tracy and C. F. Zukoski, *J. Non-Cryst. Solids*, 1988, **104**, 95–106.
53 A. P. Philipse and A. Vrij, *J. Colloid Interface Sci.*, 1989, **128**, 121–136.
54 W. Wang, B. Gu, L. Liang and W. Hamilton, *J. Phys. Chem. B*, 2003, **107**, 3400–3404.
55 J. González-Irun, A. Garcia, R. Artiaga, L. L Marzan, D. Hui and M. Chipara, *Mater. Res. Soc. Symp. Proc.*, 2006, **887**, 71–77.
56 S. Havriliak and S. Negami, *Polymer*, 1967, **8**, 161–210.
57 T. Aihara, H. Saito, T. Inoue, H.-P. Wolff and B. Stuehn, *Polymer*, 1998, **39**, 129–134.
58 J. W. Sy and J. Mijovic, *Macromolecules*, 2000, **33**, 933–946.
59 I. M. Kalogeras, A. Vassilikou-Dova and E. R. Neagu, *Mater. Res. Innovations*, 2001, **4**, 322–333.
60 M. Dionisio, A. C. Fernandes, J. F. Mano, N. T. Correia and R. C. Sousa, *Macromolecules*, 2000, **33**, 1002–1011.
61 I. M. Kalogeras and A. Vassilikou-Dova, *J. Phys. Chem. B*, 2001, **105**, 7651–7662.
62 F. Garwe, A. Schönhals, H. Lockwenz, M. Beiner, K. Schroter and E. Donth, *Macromolecules*, 1996, **29**, 247–253.
63 E. A. McGonigle, J. H. Daly, S. D. Jenkins, J. J. Liggat and R. A. Pethrick, *Macromolecules*, 2000, **33**, 480–489.
64 R. Casalini and C. M. Roland, *Phys. Rev. Lett.*, 2009, **102**, 035701.
65 K. Fukao and H. Koizumi, *Phys. Rev. E: Stat., Nonlinear, Soft Matter Phys.*, 2008, **77**, 021503.
66 G. W. Scherer, *J. Am. Ceram. Soc.*, 1986, **69**, 374–381.
67 O. S. Narayanaswamy, *J. Am. Ceram. Soc.*, 1971, **54**, 491–498.
68 R. Greiner and F. R. Schwarzl, *Rheol. Acta*, 1984, **23**, 378–395.
69 G. Power, G. P. Johari and J. K. Vij, *J. Chem. Phys.*, 2003, **119**, 435–442.
70 J. M. Hutchinson, *Prog. Polym. Sci.*, 1995, **20**, 703–760.
71 W. J. Davis and R. Pethrick, *Eur. Polym. J.*, 1998, **34**, 1747–1754.
72 F. Simon and Z. Anorg, *Z. Anorg. Allg. Chem.*, 1931, **203**, 219–227.
73 J. G. Curro, R. R. Lagasse and R. Simha, *Macromolecules*, 1982, **15**, 1621–1626.
74 D. Cangialosi, M. Wubbenhorst, H. Schut, A. van Veen and S. J. Picken, *Phys. Rev. B: Condens. Matter Mater. Phys.*, 2004, **69**, 134206.

75 L. Hu and Y. Z. Yue, *J. Phys. Chem. B*, 2008, **112**, 9053–9057.
76 K. Chen. and S. Vyazovkin, *J. Phys. Chem. B*, 2009, **113**, 4631–4635.
77 S. V. Nemilov, *Glass Phys. Chem.*, 2000, **26**, 511–530.
78 A. Serghei, H. Huth, M. Schellenberger, C. Schick and F. Kremer, *Phys. Rev. E: Stat., Nonlinear, Soft Matter Phys.*, 2005, **71**, 061801.
79 A. Serghei, H. Huth, C. Schick and F. Kremer, *Macromolecules*, 2008, **41**, 3636–3639.
80 D. Labahn, R. Mix and A. Schönhals, *Phys. Rev. E: Stat., Nonlinear, Soft Matter Phys.*, 2009, **79**, 011801.
81 B. W. Rowe, B. D. Freeman and D. R. Paul, *Polymer*, 2009, **50**, 5565–5575.